Ultrasonics 160 (2026) 107896

Contents lists available at ScienceDirect

Ultrasonics

journal homepage: www.elsevier.com/locate/ultras

System for controlled mechanical therapies of the brain

Eli Finlinson *, Matt Snyder, Tom Riis, Jan Kubanek

University of Utah Biomedical Engineering, 36 S Wasatch Dr #3100, Salt Lake City, 84112, UT, United States of America

ARTICLE INFO

Keywords:
FUS
Focused ultrasound
HIFU
High-intensity
Skull transmission
Low-frequency
Focal preservation

ABSTRACT

Transcranial focused ultrasound enables remote targeted therapies that were previously only possible using surgical approaches. Mechanical therapies are particularly attractive due to their confined action and the elimination of the potentially harmful tissue and skull heating. However, systems for controlled mechanical therapies of the brain have been missing. Here, we have developed a prototype of such a system. The system operates at a relatively low frequency of 325 kHz (bandwidth 270–380 kHz) to accentuate mechanical effects and minimize the shift of the focal point, field distortion, and acoustic attenuation. We evaluated the transcranial performance of the system through 21 *ex-vivo* human skulls. There was a favorably low shift of the focal point (mean of 1.2 mm; 2.6 mm max), a minimal increase in focal volume (mean increase of 18%), and moderate attenuation of the pressure field (average 67% pressure attenuation). These values were achieved without phase correction. These results demonstrate that systems operating at a relatively low frequency are less prone to the aberrations of ultrasound by the skull, and provide a prototype that has the potential to be used for combined neuromodulation and mechanical therapies. However, translation to clinical high-intensity applications will require further validation, including *in-vivo* thermometry and safety testing.

1. Introduction

Disorders of brain function affect nearly one in three people globally [1,2]. For many of these patients, pharmacological interventions are ineffective and produce substantial side effects [1–5]. As a result, there is a critical need for noninvasive brain therapies that can reliably reach and modulate deep neural structures. Focused ultrasound (FUS) has emerged as a promising platform for this purpose, offering noninvasive energy delivery through the intact skull. Although first clinical applications were based on thermal lesioning [6–9], mechanical therapies, whether low-intensity (neuromodulation, blood–brain barrier opening) or high-intensity (histotripsy, boiling histotripsy) are attracting attention due to a relatively sharp focus and lower risk for damage of unintended tissues compared to thermal therapies [10–15]. The low-intensity therapies are advantageous in that they are reversible, whereas high-intensity therapies minimize the need for repeated use. Low-intensity therapies also have the potential to guide high-intensity therapies through systematic evaluation of the contribution of specific brain regions to disease signs and symptoms. This dual use opens new opportunities for individualized treatments, but systems with that capacity have been missing. A system to provide effective mechanical therapies of the brain must meet criteria for effectiveness and for minimization of the aberrations by the head. Regarding effectiveness, neuromodulation [16] and cavitation-related effects (blood–brain barrier opening, local drug release [17]) are more effective at lower frequencies. Aberrations of ultrasound by the head can also be alleviated by using lower frequencies. Both ultrasound dephasing and attenuation are less severe at lower frequencies [18–21]. Thus, next-generation systems for mechanical therapies should generally operate at low frequency. At the same time, the frequency should be high-enough to provide favorable focus, e.g., on the order of individual brain nuclei such as the VIM [6], i.e., on the order of about 4 mm diameter [22,23]. Multiple large-array systems, such as Insightec's Exablate platform and those described by others [24,25], have demonstrated effective deep targeting for both thermal and low-intensity focused ultrasound (LIFU) applications. Building on this work and the above considerations, we developed a system operating at a center frequency of 325 kHz with the aim to reduce skull-induced aberration while maintaining a sufficiently small focal size for both LIFU and high-intensity (HIFU) mechanical therapies all while minimizing the need for explicit aberration correction. We evaluated the above premises in vitro and through human *ex-vivo* human skulls.

* Corresponding author.
E-mail address: u1117121@utah.edu (E. Finlinson).

https://doi.org/10.1016/j.ultras.2025.107896
Received 17 July 2025; Received in revised form 13 November 2025; Accepted 14 November 2025
Available online 29 November 2025

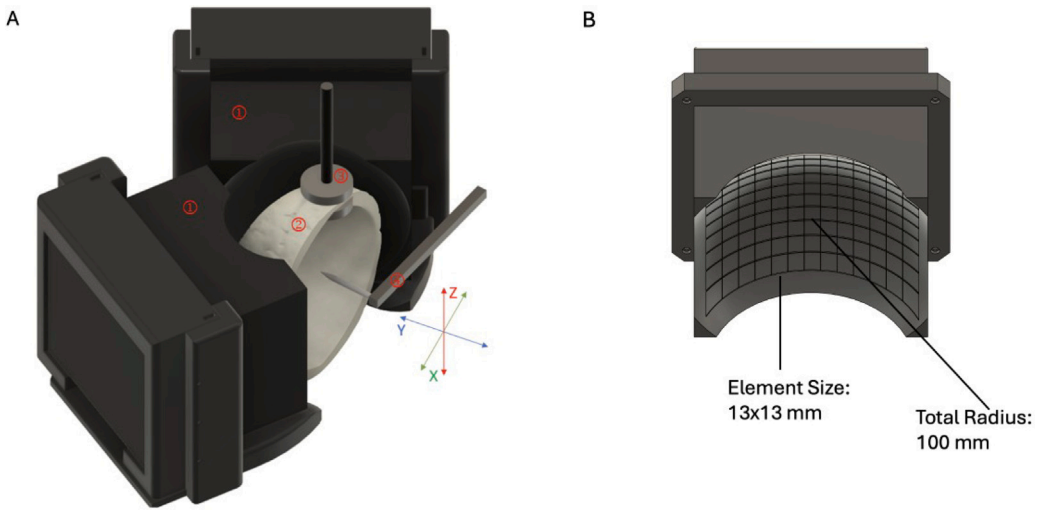

Fig. 1. System and setup. Experimental setup (A) and single transducer array (B). The experimental setup contains: (1) arrays placed in custom frame, (2) skull cap, (3) magnets securing the skull to a positioning system, (4) fiber optic hydrophone connected to a micro manipulator. Single arrays contain a 10 × 13, 13 × 13 mm square PZT elements in a spherical configuration with radius = 100 mm.

2. Methods

2.1. Overview

This study investigated the capability of a 256 hemispherical FUS array operating at 325 kHz to perform mechanical therapies through the human skull. Specifically we characterized the pressure output and steering capabilities of the array in free field as well as the attenuation, focal shift, and change in focal volume when applied through 21 *ex-vivo* human skulls (Skulls Unlimited, OK, USA).

2.2. Device specifications

Simulations performed in Field II [26,27] showed that the use of 2 large hemispherical arrays offset at an angle of 30 degrees allowed for creation of a compact focus while also enabling a geometry in which each element could possibly transmit/receive from the mirrored side for possible through transmit skull correction [28]. These simulations guided the production of manufactured two custom 128-element focused ultrasound arrays (Doppler Electronic Technologies, Guangzhou, China). Each transducer has 128 PZT elements of size 13 × 13 mm with 1 mm kerf and spherical radius of 100 mm (**Fig. S1**). The fundamental frequency of the elements is 325 kHz. These arrays were placed in a mirrored format, with a custom frame fixing the two arrays. Both arrays are simultaneous powered by the NXT-256 platform (Verasonics, WA, USA), enabling precise control over the timing and activation of individual elements. Pressure waveforms were recorded using a fiber optic hydrophone (Precision Acoustics, Dorset, UK), paired with a high-resolution digital oscilloscope (Pico Technologies, St. Neots, UK), both synchronized via the NXT-256 system. Scans were conducted in a degassed water tank using the AIMs III scanning system (Onda, CA, USA), which features an electronic micromanipulator for accurate hydrophone positioning (Fig. 1). All components were coordinated through a custom MATLAB script (MathWorks, MA, USA), ensuring synchronized transmission, acquisition, and spatial mapping of the acoustic field.

2.3. Free field experimental set-up

In order to analyze potential pressure output and steering capabilities, we performed multiple scans in free field. Peak negative pressure output of our arrays was measured via three acquisitions of 40-cycle bursts driven at voltage steps ranging from 5 to 80 V at the geometric focus of the array. Hydrophone alignment to the focus was ensured through a series of 2D scans, with the center of each subsequent scan being defined as the location of the spatial peak in the pressure distribution of the previous scan, until the focus was centered in all three planes.

To validate the pressure output, the measurements were verified with 2 other calibrated hydrophones. To avoid damage to the hydrophones, we emitted the ultrasound from individual elements separately and summed their waveforms, extracting the summed peak negative pressure as the total output of the system. This superposition is possible due to pressure being additive. Steering ability was quantified by preforming three 80 × 80 mm plane scans with a step size of 0.5 mm through the geometric center of the arrays for the XY (Coronal), XZ (Transverse), and YZ (Saggital) planes. These scans were driven at 30 V and featured 40 cycle pulses. To evaluate steering ability in each plane, a phase delay adjustment algorithm was used to align the measured waveforms at different points along each axis. Intensity fields corresponding to each steered point were calculated, peak intensity was normalized against the peak intensity found at the geometric focus. In addition to the hydrophone scans, we conducted 200 × 200 mm field simulations (**Fig. S2**) of the array output in free field. These simulations and steering scans both covered a larger field of view than was experimentally unfeasible inside the skull cavity, and were used to probe whether peripheral lobes might appear outside the 15 mm scan window that would later be used for skull measurements. This approach ensured that our chosen scan volume would capture the dominant focus and relevant side-lobes.

2.4. Skull scan experimental set-up

We performed a free-field characterization to identify the peak pressure location of the ultrasound focus (Fig. 2**A**). A 15 × 15 × 15 mm^3 volume centered on the focal point was then defined as the region of interest to balance field-of-view with skull and array geometric

constraints. The hydrophone was raster-scanned through this volume in 0.5 mm increments to construct a three-dimensional pressure field. This step size was chosen as a compromise, between spatial resolution and scan time. The array elements were driven at 30 V and emitted 10 cycle pulses, with the inter-element delay stipulated above. These scan parameters were used all subsequent skull measurements to assess changes in spatial distribution and intensity of the field, focus and side-lobes.

We prepared calvarial bone specimens by sectioning above the supraorbital ridge anteriorly and continuing posteriorly to 3–4 cm above the inion, thereby isolating the cranial vault without the facial skeleton or cranial base. Each of these *ex-vivo* skull sections were scanned under identical conditions, allowing direct comparison of field distortions between subjects (Fig. 1). Both sexes were represented, and the skulls spanned a range of ages, although only Caucasian samples were available. Prior to scanning, all skulls were submerged in water and degassed at 25 mmHg for at least 12 h to eliminate trapped air following methods in similar studies [19,20,29,30]. For positioning, we identified the widest lateral and anterior–posterior dimensions of each skull and aligned with a removable 5 cm pointer, positioned at the intersection of these dimensions within the skull cavity, to the focus identified in free field as marked by the starting position of the hydrophone. This protocol enabled reproducible alignment and consistent reconstruction of the pressure field under both free-field and transcranial conditions, facilitating direct evaluation of skull-induced effects on focal quality and intensity.

2.5. Data analysis

As a metric for determining the effects of low-frequency ultrasound at penetrating the skull we analyzed the change in peak pressure and intensity, the shift of the focus location and the change in the focal volume. Waveform data were processed using a custom MATLAB script. We calculated and averaged negative peak pressure as well as intensity across all skulls and normalized them. We calculated peak shift by comparing and averaging the euclidean distance between free field and the skull scans. As a measure of focal volume, we devised a binary mask of voxels that exceed half of the max intensity, including any voxels from both the main and side lobes, of the field as follows:

$$\int_{xyz} [I_{x,y,z} > \frac{I_{max}}{2}] dx dy dz$$

Total focal volume change was then calculated by comparing the focal volume of free field with that of the skull scans. In addition to the above, we separated the pressure losses into contributions from attenuation versus aberration. We compared the emitted individual element waveform amplitude and phase at the geometric focus to that of the its free field counter part. From these values, attenuation was estimated as the reduction in average waveform amplitude relative to free field, while aberration was estimated as the residual pressure loss due to destructive interference following phase misalignment. This approach allowed us to quantify the relative impact of material absorption/scattering versus phase distortion. Furthermore, using skull donor sex and age, we performed multiple linear regression (with age as a continuous covariate and sex as a categorical factor, i.e. an ANCOVA model) to assess demographic effects on acoustic transmission.

3. Results

3.1. Focusing capacity

We first characterized the focusing capacity of the system. To do so, we focused the ultrasound into the geometric center of the two arrays, and characterized the emitted pressure field using a hydrophone. The fundamental frequency of 325 kHz produced confined fields (Fig. 2**a**), with full-width-half-maximum (FWHM) diameters of 6 mm, 3 mm, and 3 mm in the X, Y, and Z dimensions, respectively. This FWHM region encompasses the full main lobe and the first side lobe, thereby capturing the total region of effect. The characterization of the fields obtained in each skull is shown in **Figs. S5-S24**.

We then evaluated the system's pressure output. The system elicits peak negative pressures at the focus of 0–35 MPa for driving inputs ranging from 0–80 V in amplitude with further ability to drive past 100 V. There was a saturating relationship between the output and the input, with a relationship following the formula $P = -0.002V^2 + 0.602V - 0.519$ (Fig. 3) where P is output peak negative pressure (MPa) and V is the input voltage. The saturation of output pressure with increasing drive voltage likely indicates a change in the impedance of individual FUS elements.

We assessed the system's electronic steering range in all dimensions. The maximum steering range that maintained half of maximum intensity was ±25 mm in the medial–lateral direction, $+16, -17$ mm in the dorsal–ventral direction, and ±14 mm in the anterior–posterior direction (Fig. 4). Across the steering range shown in Fig. 4, we found that the convex hull, which estimates the size of the main lobe, decreased by a maximum of 18%, indicating a slight reduction in focal size at the steering maxima. For increased steering range, the subject's head can be positioned in predefined locations with respect to the arrays.

3.2. Transcranial application: Attenuation

We subsequently introduced *ex-vivo* human skulls within the path of the emitted ultrasound. To determine the effect of each skull on the ultrasound transmission, we compared focal peak negative pressure and intensity across skull scans normalized to the free-field condition. On average, the skulls attenuated peak negative pressure by 67%, with values ranging from 50% to 80% (Fig. 5**a**), and attenuated acoustic intensity by 87% on average, with a range of 65% to 95% (Fig. 5**b**). Across skulls, attenuation accounted for approximately 95% of the total transmission loss on average, while aberration accounted for the remaining 5% (Fig. 6). Although both mechanisms reduced transmitted pressure, attenuation was the dominant contributor. The relative contributions were consistent across the skulls, with some inter-subject variability ($std = \pm 3\%$).

We examined whether skull donor age or sex influenced the pressure transmitted through the skull (Fig. 7). A multiple linear regression model revealed a positive trend between age and transmitted pressure ($\beta = 0.044$ MPa/year), though the effect did not reach significance ($F(1, 18) = 3.93$, $p = 0.063$). A Pearson correlation between age and pressure did, however, indicate a modest, statistically significant relationship ($r = 0.46$, $p = 0.035$), suggesting that older skulls may attenuate less (Fig. 7**a**). Sex did not have significant leverage on the pressure transmission ($F(1, 18) = 1.53$, $p = 0.23$) either, with male skulls transmitting slightly less pressure on average −0.60 MPa than female skulls (Fig. 7**b**). The model explained 27.4% of the variance in transmitted pressure ($R^2 = 0.274$).

3.3. Transcranial application: Focal shift and volume

We next characterized the shift in focal coordinates following the introduction of each skull in the ultrasound path (Fig. 8). There was an average 1.2±0.5 mm total shift away from the free-field focus (range 0.5 to 2.6 mm). This value was significantly different from zero (one-sided t-test, $t\_20 = 9.75, p < 0.001$. Fig. 8 shows that largest displacement was observed along the Y-axis (dorsal–ventral; mean of 0.7 mm), with minimal shifts along the X (−0.02 mm) and Z (0.07 mm) directions. This axis showed a consistent bias across skulls, whereas X and Z shifts remained minimal despite greater opportunity for positioning variability in these directions during repeated mounting. Of these shifts, the shift in the Y direction was significantly different from zero (two-sided t-test $t\_20 = 3.62$, $p = 0.002$), while the shifts in the X ($t\_20 = -0.29$, $p = 0.771$) and Z ($t\_20 = 0.57$, $p = 0.576$) directions were not.

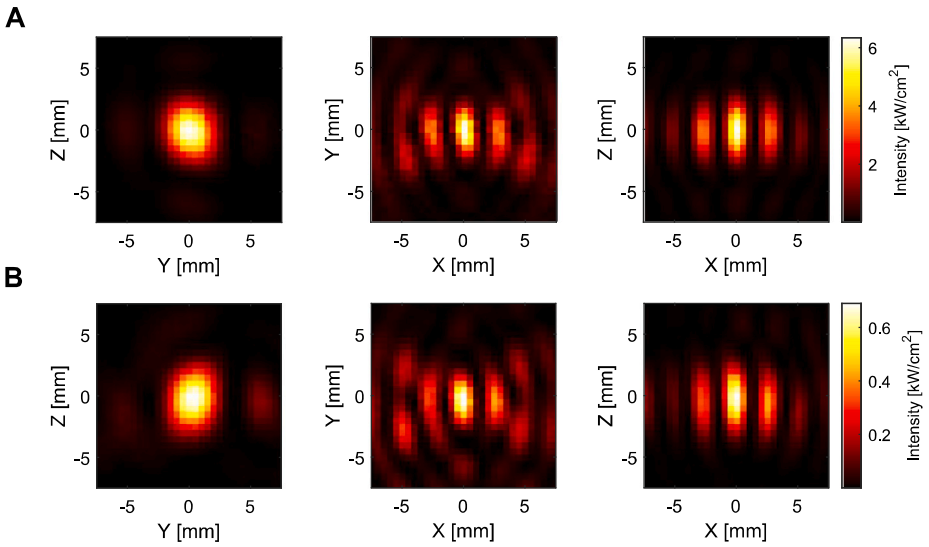

Fig. 2. Focusing capacity of the system. Orthogonal slices through the acoustic intensity field measured in free field (A) and after transcranial propagation through a sample human skull (B) at 30 V input. Each shows sagittal (YZ), coronal (XY), and transverse (XZ) slices respectively centered at the acoustic focus.

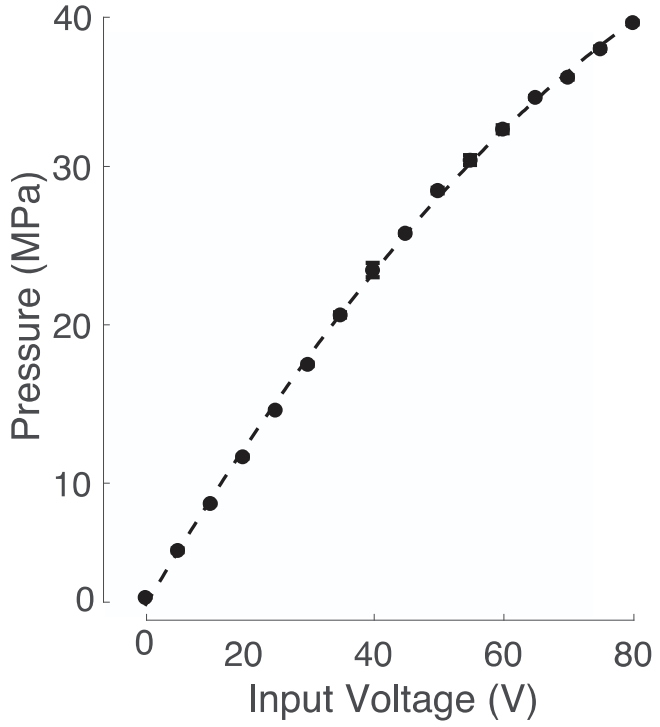

Fig. 3. Pressure output. Peak negative pressure output at the geometric focus as a function of the input voltage. The measurements were performed in free field. The dashed line constitutes a quadratic polynomial fit.

Fig. S3 shows component-wise absolute shift and **Fig. S4** shows axial line plots that visualize these shifts. The discrete appearance of the distributions reflects the 0.5 mm sampling step used in the raster scans, which imposes a maximum localization uncertainty of ±0.25 mm per axis. This quantization is small relative to the observed Y-axis bias and mean total shift, and therefore does not affect the reported conclusions

Furthermore, we analyzed the change in focal volume following the introduction of the *ex-vivo* skulls within the ultrasound pathway (Fig. 9). When comparing transcranial to free field we found an increase in focal volume of $18 \pm 35\%$ (mean ± s.d.). Inspection of orthogonal slices across skulls (**Figs. S5–S25**) suggests that the overall focus geometry was qualitatively preserved. However, because side lobes intermittently exceeded the half-maximum threshold, conventional axis-by-axis FWHM analysis did not provide a reliable or interpretable measure of focal shape. For this reason, we focused on focal volume as the primary quantitative descriptor.

4. Discussion

4.1. Summary of results

In this study, we evaluated the possibility of using a low-frequency device prototype for mechanical therapies of the brain. We assessed the effects of human skulls on key parameters of the ultrasound propagation. We also evaluated output characteristics of a device prototype. Across 21 human *ex-vivo* skulls, we observed an average focal shift of approximately 1.1 mm and a focal volume increase of only about 17%. These values compare favorably to previous studies (see Table 1) [30–32]. Thus, low-frequency operation helps to minimize the distortions induced by the skull. Despite the improved focusing characteristics, we observed significant transmission loss: on average, the transmitted pressure was reduced by 67% from free-field values. These values are consistent with, but slightly higher than, prior attenuation measurements in the 300–400 kHz range, which typically report pressure reductions between 50% and 60% depending on skull thickness and orientation [30–32]. We observed a consistent bias toward dorsal–ventral (Y axis) displacement. The effect was likely due to refraction from the skulls because it was observed specifically and consistently for Y and not for the X and Z axes. In examining demographic contributors to variability, we found no statistically significant difference in transmission efficiency between male and female skulls. However, a modest positive correlation was observed between donor age and transmitted pressure. This trend may reflect age-related changes in bone structure, including reduced cortical density or increased porosity, which have been previously linked to decreased ultrasound attenuation [33].

4.2. Comparison to prior literature

Our results reinforce and extend prior observations regarding the effects of the human skull on focused ultrasound transmission, while addressing notable gaps in the experimental literature concerning low-frequency operation. Numerous studies have established that transcranial ultrasound at higher frequencies (≥500 kHz) suffers from severe

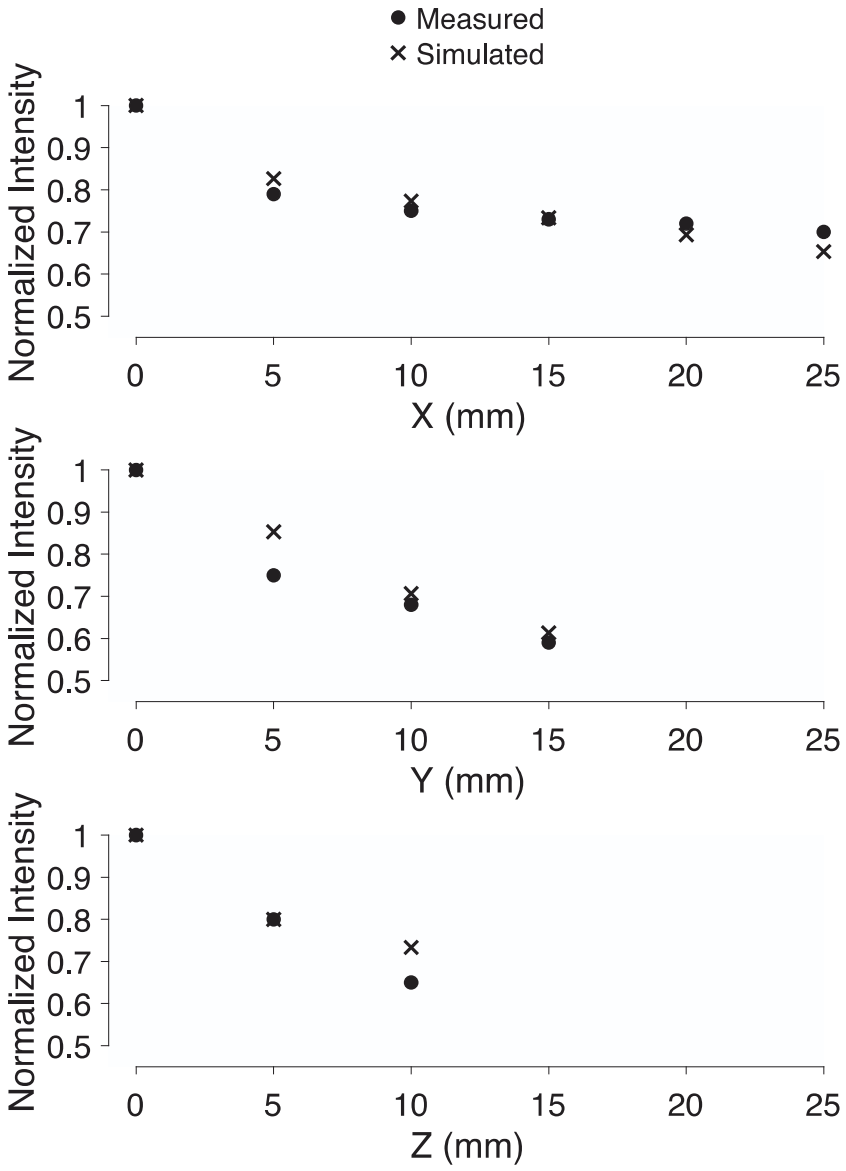

Fig. 4. Electronic steering capacity. Steering extent in each direction from the geometric focus (ΔX : medial–lateral, ΔY : dorsal–ventral, ΔZ : anterior–posterior). Normalized intensity with respect to the intensity at the geometric focus is shown. Measured values of intensity loss are compared to simulated values and values are plotted until they fall below half of the max intensity found at the geometric focus. Steering was evaluated in both directions along each axis. Because of array asymmetry along the Y-axis, only dorsal steering is plotted, with ventral steering extending slightly further.

Table 1
Effects of frequency on transcranial transmission. Focal shift, attenuation, and focal volume change for studies that evaluated transcranial transmission with no correction algorithms.

Study	Leung et al. ($n = 3$)	Clement et al. ($n = 10$)	Li et al. ($n = 10$)	Li et al. ($n = 10$)	Krokhmal et al. ($n = 4$)	Our study ($n = 21$)
Carrier frequency (kHz)	670	740	650	1000	270	325
Pressure attenuation (%)	50 ± 13	66 ± 20	67 ± 16	76 ± 18	62	66 ± 5
Focal shift (mm)	1.0 ± 0.34	1.1 ± 0.64	1.1 ± 1.10	0.9 ± 1.20	1.9	1.1 ± 0.5
Focal volume increase (%)	200 ± 100	100 ± 40	40 ± 30	40 ± 40	35	17 ± 35

attenuation and focal distortion, often resulting in focal shifts exceeding 3 mm and reductions in transmitted pressure well beyond 70% in the absence of phase correction strategies [20,30,32]. Our use of 325 kHz FUS resulted in a mean focal shift of 1.1 mm and a pressure attenuation of approximately 67%, demonstrating similar preservation of focus compared to higher-frequency studies, despite the absence of aberration correction. The attenuation levels we observed are comparable to those reported by White et al. who found that skull-induced attenuation

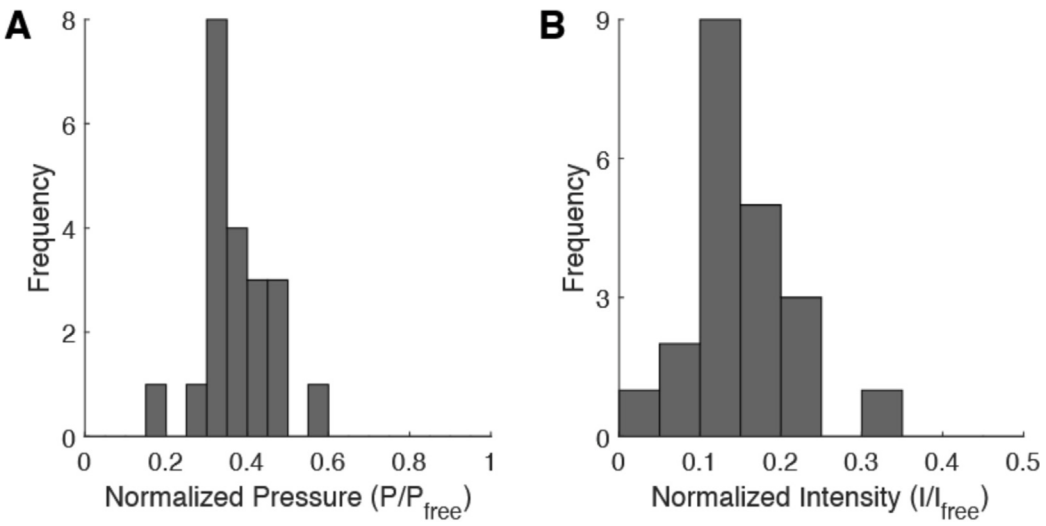

Fig. 5. Ultrasound attenuation through *ex-vivo* skulls at 325 kHz. Histograms of the distribution of (A) normalized pressure, and (B) normalized intensity through *ex-vivo* human skulls ($n = 21$) relative to free-field measurements.

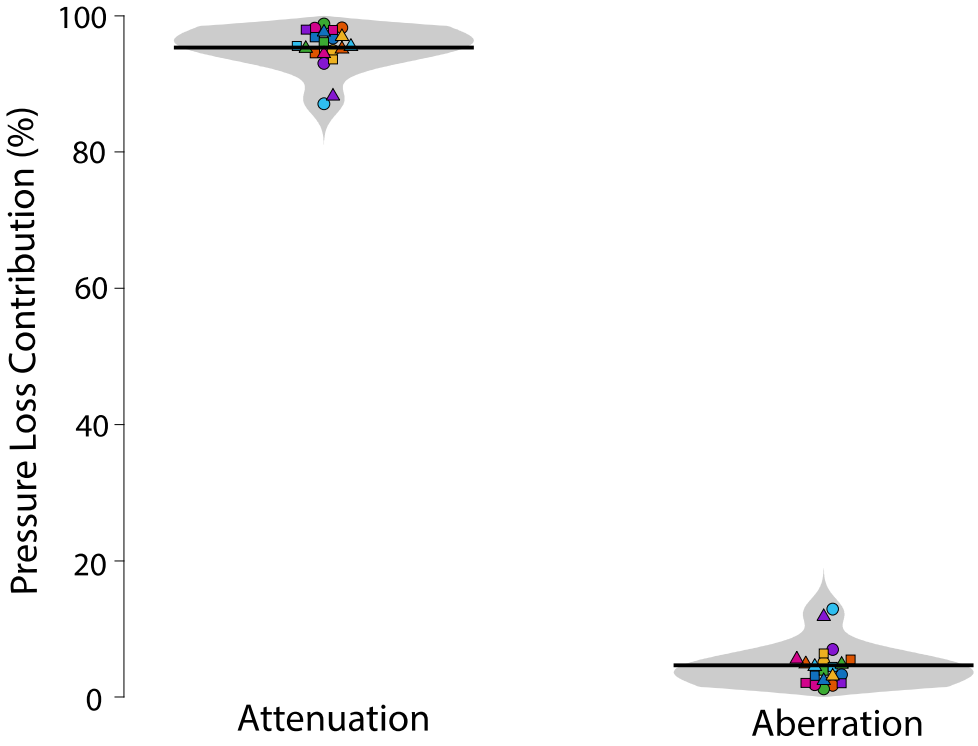

Fig. 6. Percent pressure loss due to Attenuation vs. Aberration. Violin plots showing the amount of pressure loss through the skull caused by attenuation and aberration when individual elements were compared to free field. Average pressure loss due to attenuation was found to be $95 \pm 3\%$.

is markedly lower at 300–400 kHz than at 500 kHz and above [20]. Pinton et al. further showed that lowering the frequency to the 300–400 kHz range increases the transmission efficiency through both temporal and parietal bone, with average pressure transmission coefficients increasing by 30%–50% relative to 650 kHz [34,35]. Our findings directly corroborate these trends, confirming that low-frequency ultrasound can maintain sufficient acoustic intensity for transcranial therapies. At 325 kHz, the focal volume increased on average only be 17%. This compares favorably to the more substantial increases reported by Younan et al. [36] at 650 kHz and by Clement and Hynynen [12,36] at 1 MHz, both of whom noted dramatic losses in spatial precision in the absence of a correction. This suggests that the lower-frequency regime provides a more robust focus for transcranial applications, even without a correction (Table 1). This also corresponds with the findings of Krokhmal et al. who found that lower frequencies (250 and 500 kHz) minimized the shift of the focal point [21]. Few studies have systematically assessed inter-skull variability at lower frequencies. Li et al. reported that anatomical differences among skulls introduce significant variance in both attenuation and focus, yet found that low-frequency ultrasound (300–400 kHz) reduced this variability [32]. Our results are in agreement with these observations, and support the feasibility of clinical protocols that do not require complex compensation algorithms. By separating transmission losses into attenuation versus aberration, we found that attenuation within the skull bone accounted for the majority of the pressure reduction, with aberration contributing

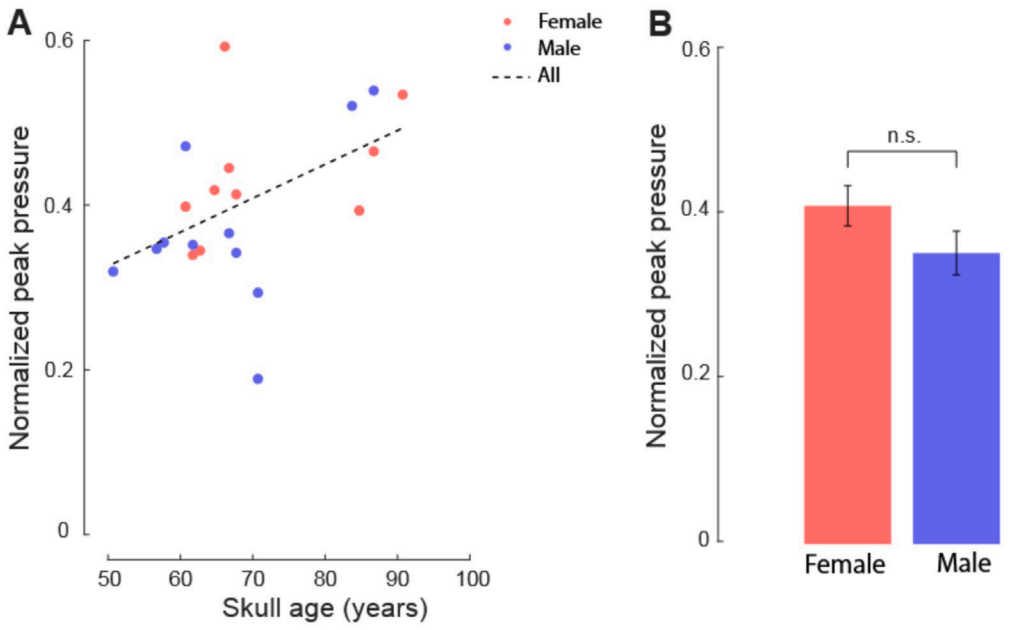

Fig. 7. Normalized spatial peak negative pressure based off of skull demographic data. (A) Normalized spatial peak negative pressure as a function of skull donor age ($p = 0.035$). (B) Mean ± SEM of normalized spatial peak negative pressure for male and female skulls.

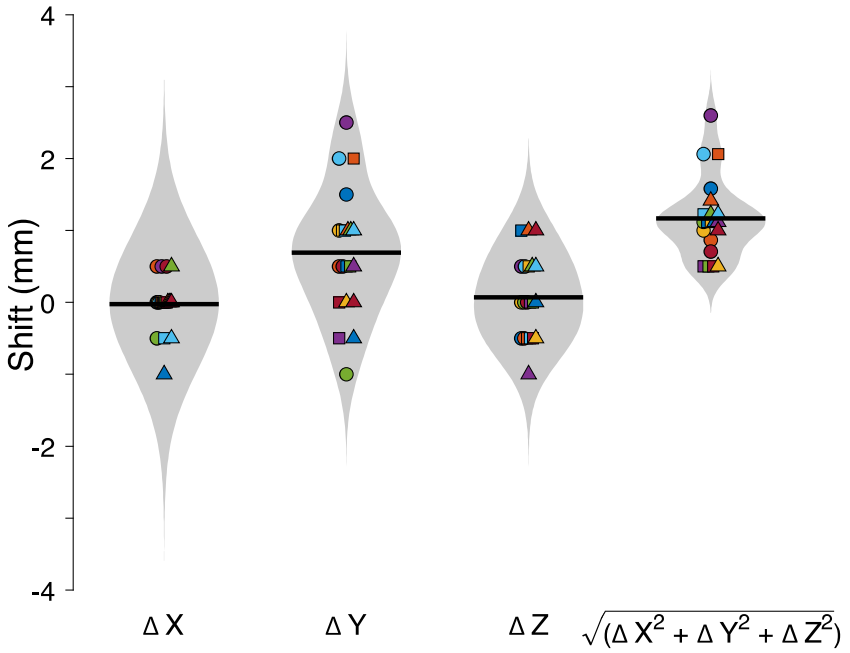

Fig. 8. Focusing ability through human skulls. Distribution of focal shift across individual skulls and directions. The violin plots show the displacement along each axis (ΔX : medial–lateral, ΔY : dorsal–ventral, ΔZ : anterior–posterior) as well as length of the vector shift. Colored points represent individual skulls. Thick black lines denote the median of each distribution.

a smaller fraction. This pattern is consistent with prior reports that attenuation dominates at lower frequencies [20,35], whereas aberration effects become increasingly problematic at higher frequencies. These findings suggest that further improvements in transmission efficiency at 325 kHz will likely require strategies to reduce effective bone path length or exploit skull windows, rather than relying solely on phase correction.

In addition to prior *ex-vivo* skull transmission studies, Xu et al. (2014) [37] examined the effects of a 220 kHz ExAblate Neuro system *in-vivo* in piglets. Their work established thresholds for producing either thermal lesions (≥53–55 °C with long-duration sonications at 140–300 W) or hemorrhagic mechanical lesions (20 s sonications at 300–700 W) and identified a cavitation dose threshold (õ.09 V Hz) beyond which hemorrhage occurred. Importantly, these experiments were performed following craniectomy, and thus did not address the

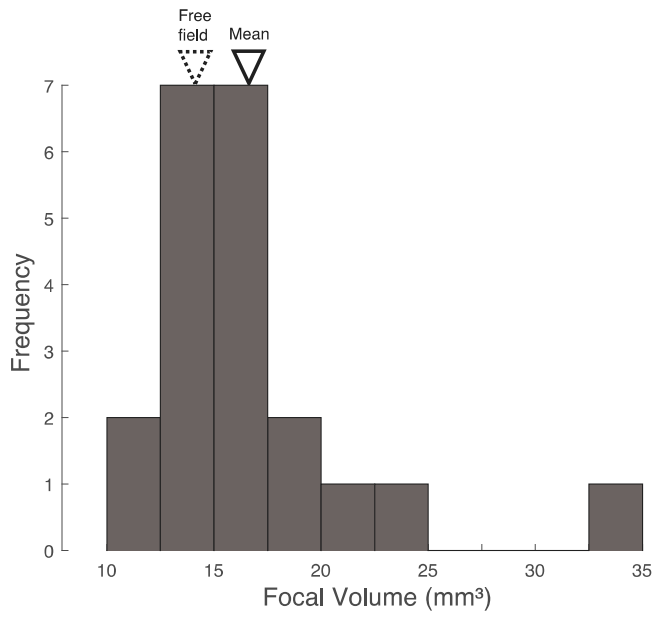

Fig. 9. Skull effects on focal volume. Histogram of the focal volume inside each skull. The dashed triangle shows focal volume obtained in free field, and the solid triangle denotes the mean.

impact of the skull on focal shift, volume, or transmission. By contrast, the present study directly quantifies these transcranial effects across 21 intact human skulls. Our results therefore complement Xu et al. by extending low-frequency characterization from lesion safety thresholds to the specific distortions and attenuations introduced by the skull barrier.

Collectively, these direct comparisons highlight the principal advantage of low-frequency FUS for transcranial applications: robust transmission with modest focal distortion, even in the absence of correction. By extending these findings to a larger and more diverse skull sample, our work helps establish the 300–400 kHz range as a practical operating window for future systems harnessing mechanical effects.

4.3. System output

The prototype system evaluated in this study could in principle be used for a wide set of transcranial therapies. The system can drive low-intensity applications (Fig. 3) and can also power high-intensity applications (Fig. 3), up to about 35 MPa in free field. This field strength is on the order of that required for histotripsy [11,14,38], and can be increased further by increasing the driving voltage. The use of relatively low frequency further facilitates the production of mechanical effects. We observed that the bulk of the pressure loss through the skull was due to attenuation rather than dephasing (Fig. 6). This raises the possibility that using lower frequencies may obviate the need for correction of phase, and thus the associated CT or MRI scans of the head. Nonetheless, our data show that dephasing still constitutes a significant, albeit not substantial, factor, and so correcting for dephasing may be desirable for specific applications.

The system can support steering range of about ±25 mm in the medial–lateral direction, ±17 mm in the dorsal–ventral direction, and ±14 mm in the anterior-posterior direction (Fig. 4). This treatment envelope can be further broadened by manual adjustment of the head location with respect to the arrays. We note that our method assumes linear acoustic propagation when summing individual element waveforms. Nonlinear propagation effects, which become more significant at high pressures, are therefore not captured here. As such, the reported pressure values should be interpreted as upper-bound estimate of the total output. At the highest drive levels, nonlinearities and saturation effects are expected to gradually limit increasing pressure [39,40]. Further investigation will be required to characterize HIFU effects under realistic conditions.

4.4. Limitations

This device is a prototype and has certain limitations and testing that must be resolved before translation to human treatment. First, we characterized the system output but have not directly tested its capacity for applications such as histotripsy. Furthermore, many studies highlight important benchmarks and limitations of HIFU devices [21,41–43]. Future studies will ensure that HIFU ablation size, and targeting comply with these benchmarks and ensure patient safety. Current pursuits by the authors to ensure clinical feasibility include verification of targeting through use of MRI thermometry and classification of lesion size in *ex-vivo* tissue. Second, the system described in this study constitutes an early prototype of the potential system used in the clinics. There are many variables that would need to be controlled, including systems for head positioning, ultrasound coupling, and treatment monitoring. Future research could consider approaches such as the angular spectrum method to reduce scan time and improve resolution [44,45]. Skulls were degassed similarly as in previous studies. Future studies may validate that degassing was complete using imaging methods such as CT.

4.5. Summary

In summary, we have evaluated the feasibility of an approach and a prototype system for mechanical therapies of the brain using transcranial focused ultrasound. Operating at low frequency, the approach facilitates the focusing of ultrasound through the head and the induction of mechanical effects. The resulting systems could be used for several therapies, including neuromodulation, blood–brain barrier opening, local drug release, and histotripsy, in separation or combined. For instance, systematic, transient neuromodulation could be used to guide more permanent histotripsy treatments. Such approaches could realize the potential of the ultrasonic technology for individualized, circuit-directed treatments of mental and neurological disorders.

CRediT authorship contribution statement

Eli Finlinson: Writing – review & editing, Writing – original draft, Visualization, Validation, Software, Resources, Project administration, Methodology, Investigation, Formal analysis, Data curation, Conceptualization. **Matt Snyder:** Writing – review & editing, Writing – original draft, Validation, Software, Resources, Methodology, Investigation, Formal analysis. **Tom Riis:** Validation, Supervision, Software. **Jan Kubanek:** Writing – review & editing, Visualization, Validation, Supervision, Funding acquisition.

Declaration of competing interest

The authors declare that they have no known competing financial interests or personal relationships that could have appeared to influence the work reported in this paper.

Acknowledgments

This research is supported by NIH, United States RF1NS128569 and NSF DARE, United States. The authors acknowledge the use of artificial intelligence writing tools to assist in reviewing and editing the text of this manuscript for clarity and readability. The authors reviewed and take full responsibility for the content of the manuscript.

Appendix A. Supplementary data

Supplementary material related to this article can be found online at https://doi.org/10.1016/j.ultras.2025.107896.

Data availability

Data will be made available on request.

References

[1] Disease Control Priorities Related to Mental, Neurological, Developmental and Substance Abuse Disorders, World Health Organization, 2006, Google-Books-ID: zsVMBTF8vREC.

[2] R.M. Berman, M. Narasimhan, D.S. Charney, Treat.-Refract. Depression, Defin. Charact. Depression Anxiety 5 (4) (1997) 154–164, http://dx.doi.org/10.1002/(SICI)1520-6394(1997)5:4<154::AID-DA2>3.0.CO;2-D, URL https://onlinelibrary.wiley.com/doi/abs/10.1002/%28SICI%291520-6394%281997%295%3A4%3C154%3A%3AAID-DA2%3E3.0.CO%3B2-D. _eprint: https://onlinelibrary.wiley.com/doi/pdf/10.1002/%28SICI%291520-6394%281997%295%3A4%3C154%3A%3AAID-DA2%3E3.0.CO%3B2-D.

[3] J.A. French, Refract. Epilepsy Clin. Overv. Epilepsia (2007) URL https://onlinelibrary.wiley.com/doi/full/10.1111/j.1528-1167.2007.00992.x?casa_token=XRAKRrsRAaUAAAAA%3AfBUzALd7sO9JYMHxwWJ7tVahry0B-c95dN1rOwzzz60rfEAYX50O9uv3-fCnWZ4duhY7frvnNxhCOD4.

[4] V.L. Feigin, T. Vos, E. Nichols, M.O. Owolabi, W.M. Carroll, M. Dichgans, G. Deuschl, P. Parmar, M. Brainin, C. Murray, The global burden of neurological disorders: translating evidence into policy, Lancet Neurol. 19 (3) (2020) 255–265, http://dx.doi.org/10.1016/S1474-4422(19)30411-9, URL https://www.ncbi.nlm.nih.gov/pmc/articles/PMC9945815/.

[5] A.M. Lesenskyj, M.P. Samples, J.M. Farmer, C.R. Maxwell, Treating refractory depression in Parkinson's disease: a meta-analysis of transcranial magnetic stimulation, Transl. Neurodegener. 7 (1) (2018) 8, http://dx.doi.org/10.1186/s40035-018-0113-0.

[6] W.J. Elias, N. Lipsman, W.G. Ondo, P. Ghanouni, Y.G. Kim, W. Lee, M. Schwartz, K. Hynynen, A.M. Lozano, B.B. Shah, D. Huss, R.F. Dallapiazza, R. Gwinn, J. Witt, S. Ro, H.M. Eisenberg, P.S. Fishman, D. Gandhi, C.H. Halpern, R. Chuang, K.B. Pauly, T.S. Tierney, M.T. Hayes, G.R. Cosgrove, T. Yamaguchi, K. Abe, T. Taira, J.W. Chang, A randomized trial of focused ultrasound thalamotomy for essential tremor, N. Engl. J. Med. 375 (8) (2016) 730–739, http://dx.doi.org/10.1056/NEJMoa1600159, URL https://www.nejm.org/doi/full/10.1056/NEJMoa1600159. Publisher: Massachusetts Medical Society _eprint: https://www.nejm.org/doi/pdf/10.1056/NEJMoa1600159.

[7] Y. Meng, K. Hynynen, N. Lipsman, Applications of focused ultrasound in the brain: from thermoablation to drug delivery, Nat. Rev. Neurol. 17 (1) (2021) 7–22, http://dx.doi.org/10.1038/s41582-020-00418-z.

[8] A. Fomenko, A.M. Lozano, Neuromodulation and ablation with focused ultrasound – toward the future of noninvasive brain therapy, Neural Regen. Res. 14 (9) (2019) 1509, http://dx.doi.org/10.4103/1673-5374.255961, URL https://journals.lww.com/nrronline/fulltext/2019/14090/Neuromodulation_and_ablation_with_focused.8.aspx.

[9] A. Franzini, S. Moosa, F. Prada, W.J. Elias, Ultrasound ablation in neurosurgery: Current clinical applications and future perspectives, Neurosurgery 87 (1) (2020) 1, http://dx.doi.org/10.1093/neuros/nyz407, URL https://journals.lww.com/neurosurgery/fulltext/2020/07000/ultrasound_ablation_in_neurosurgery_current.1.aspx.

[10] T.P. Kaovasia, S. Duclos, D. Gupta, K. Kalayeh, M. Fabiilli, D.C. Noll, J. Sukovich, A. Pandey, Z. Xu, T.L. Hall, A pre-clinical MRI-guided all-in-one focused ultrasound system for murine brain studies, Sci. Rep. 15 (1) (2025) 144, http://dx.doi.org/10.1038/s41598-024-84078-9, URL https://www.nature.com/articles/s41598-024-84078-9. Publisher: Nature Publishing Group.

[11] E. Vlaisavljevich, K.-W. Lin, M.T. Warnez, R. Singh, L. Mancia, A.J. Putnam, E. Johnsen, C. Cain, Z. Xu, Effects of tissue stiffness, ultrasound frequency, and pressure on histotripsy-induced cavitation bubble behavior, Phys. Med. Biol. 60 (6) (2015) 2271–2292, http://dx.doi.org/10.1088/0031-9155/60/6/2271, URL https://iopscience.iop.org/article/10.1088/0031-9155/60/6/2271.

[12] K. Hynynen, J. Sun, Trans-skull ultrasound therapy: the feasibility of using image-derived skull thickness information to correct the phase distortion, IEEE Trans. Ultrason. Ferroelectr. Freq. Control 46 (3) (1999) 752–755, http://dx.doi.org/10.1109/58.764862, URL https://ieeexplore.ieee.org/abstract/document/764862.

[13] J.R. Sukovich, Z. Xu, Y. Kim, H. Cao, T.-S. Nguyen, A.S. Pandey, T.L. Hall, C.A. Cain, Targeted lesion generation through the skull without aberration correction using histotripsy, IEEE Trans. Ultrason. Ferroelectr. Freq. Control 63 (5) (2016) 671–682, http://dx.doi.org/10.1109/TUFFC.2016.2531504, URL https://ieeexplore.ieee.org/abstract/document/7410085.

[14] J.R. Sukovich, C.A. Cain, A.S. Pandey, N. Chaudhary, S. Camelo-Piragua, S.P. Allen, T.L. Hall, J. Snell, Z. Xu, J.M. Cannata, D. Teofilovic, J.A. Bertolina, N. Kassell, Z. Xu, In vivo histotripsy brain treatment, J. Neurosurg. 131 (4) (2018) 1331–1338, http://dx.doi.org/10.3171/2018.4.JNS172652, URL https://www.ncbi.nlm.nih.gov/pmc/articles/PMC6925659/.

[15] L. Ruger, M. Langman, R. Farrell, J.H. Rossmeisl, F. Prada, E. Vlaisavljevich, Ultrasound-guided mechanical high-intensity focused ultrasound (histotripsy) through an acoustically permeable polyolefin-based cranioplasty device, IEEE Trans. Biomed. Eng. 71 (10) (2024) 2877–2888, http://dx.doi.org/10.1109/TBME.2024.3399688, URL https://ieeexplore.ieee.org/abstract/document/10528862.

[16] T. Riis, J. Kubanek, Effective ultrasonic stimulation in human peripheral nervous system, IEEE Trans. Biomed. Eng. (1) (2022) 15–22, http://dx.doi.org/10.1109/TBME.2021.3085170, URL https://ieeexplore.ieee.org/abstract/document/9444635.

[17] M.G. Wilson, A. Parikh, A. Dara, A. Beaver, J. Kubanek, Targeted drug release from stable and safe ultrasound-sensitive nanocarriers, 2024, http://dx.doi.org/10.1101/2021.12.14.471689, URL https://www.biorxiv.org/content/10.1101/2021.12.14.471689v8. Pages: 2021.12.14.471689 Section: New Results.

[18] S. Gupta, M. Mudhafar, Y.D. Borole, V. Mahalakshmi, J.V.N. Ramesh, M.A. Khan, Optimizing transcranial focused ultrasound parameters: A methodological advancement in non-invasive brain stimulation for next-gen clinical applications, Neurosci. Inform. 5 (2) (2025) 100204, http://dx.doi.org/10.1016/j.neuri.2025.100204, URL https://www.sciencedirect.com/science/article/pii/S2772528625000196.

[19] S. Pichardo, V.W. Sin, K. Hynynen, Multi-frequency characterization of the speed of sound and attenuation coefficient for longitudinal transmission of freshly excised human skulls, Phys. Med. Biol. 56 (1) (2011) 219–250, http://dx.doi.org/10.1088/0031-9155/56/1/014.

[20] P.J. White, G.T. Clement, K. Hynynen, Longitudinal and shear mode ultrasound propagation in human skull bone, Ultrasound Med. Biol. 32 (7) (2006) 1085–1096, http://dx.doi.org/10.1016/j.ultrasmedbio.2006.03.015.

[21] A. Krokhmal, I.C. Simcock, B.E. Treeby, E. Martin, A comparative study of experimental and simulated ultrasound beam propagation through cranial bones, Phys. Med. Biol. 70 (2) (2025) 025007, http://dx.doi.org/10.1088/1361-6560/ada19d.

[22] T. Hirai, C. Ohye, Y. Nagaseki, M. Matsumura, Cytometric analysis of the thalamic ventralis intermedius nucleus in humans, J. Neurophysiol. 61 (3) (1989) 478–487, http://dx.doi.org/10.1152/jn.1989.61.3.478, URL https://journals.physiology.org/doi/abs/10.1152/jn.1989.61.3.478. Publisher: American Physiological Society.

[23] J.H. Su, E.Y. Choi, K.B. Pauly, P. Ghanouni, B.K. Rutt, Improved vim targeting for focused ultrasound ablation treatment of essential tremor: A probabilistic and patient-specific approach. URL https://onlinelibrary.wiley.com/doi/full/10.1002/hbm.25157.

[24] E. Martin, M. Roberts, I.F. Grigoras, O. Wright, T. Nandi, S.W. Rieger, J. Campbell, T. den Boer, B.T. Cox, C.J. Stagg, B.E. Treeby, Ultrasound system for precise neuromodulation of human deep brain circuits, Nat. Commun. 16 (1) (2025) 1–14, http://dx.doi.org/10.1038/s41467-025-63020-1.

[25] D. McMahon, K. Hynynen, et al., Investigation of sonication parameters for large-volume focused ultrasound-mediated blood–brain barrier permeability enhancement using a clinical-prototype hemispherical phased array, Pharmaceutics 16 (10) (2024) 1289, http://dx.doi.org/10.3390/pharmaceutics16101289.

[26] J.A. Jensen, N.B. Svendsen, Calculation of pressure fields from arbitrarily shaped, apodized, and excited ultrasound transducers, IEEE Trans. Ultrason. Ferroelectr. Freq. Control 39 (2) (1992) 262–267, http://dx.doi.org/10.1109/58.139123.

[27] J.A. Jensen, FIELD: A program for simulating ultrasound systems, in: Proceedings of the 10th Nordic-Baltic Conference on Biomedical Imaging, vol. 34, (Supplement 1, Part 1) 1996, pp. 351–353.

[28] T. Riis, D. Feldman, A. Losser, B. Mickey, J. Kubanek, Device for multifocal delivery of ultrasound into Deep Brain Regions in humans, IEEE Trans. Biomed. Eng. 71 (2) (2024) 660–668, http://dx.doi.org/10.1109/TBME.2023.3313987.

[29] M.G. Wilson, T.S. Riis, J. Kubanek, Controlled ultrasonic interventions through the human skull, Front. Hum. Neurosci. 18 (2024) http://dx.doi.org/10.3389/fnhum.2024.1412921, URL https://www.frontiersin.org/journals/human-neuroscience/articles/10.3389/fnhum.2024.1412921.

[30] G.T. Clement, K. Hynynen, Correlation of ultrasound phase with physical skull properties, Ultrasound Med. Biol. 28 (5) (2002) 617–624, http://dx.doi.org/10.1016/S0301-5629(02)00503-3, URL https://www.sciencedirect.com/science/article/pii/S0301562902005033.

[31] S.A. Leung, D. Moore, T.D. Webb, J. Snell, P. Ghanouni, K. Butts Pauly, Transcranial focused ultrasound phase correction using the hybrid angular spectrum method, Sci. Rep. 11 (1) (2021) 6532, http://dx.doi.org/10.1038/s41598-021-85535-5, URL https://www.nature.com/articles/s41598-021-85535-5. Publisher: Nature Publishing Group.

[32] H. Li, I. Barnard, T. Halliwell, X. Zhang, A. Melzer, Z. Huang, Effects of skull properties on continuous-wave transcranial focused ultrasound transmission, J. Acoust. Soc. Am. 157 (4) (2025) 2336–2349, http://dx.doi.org/10.1121/10.0036344.

[33] U. Vyas, P. Ghanouni, C.H. Halpern, J. Elias, K.B. Pauly, Predicting variation in subject thermal response during transcranial magnetic resonance guided focused ultrasound surgery: Comparison in seventeen subject datasets, Med. Phys. 43 (9) (2016) 5170–5180, http://dx.doi.org/10.1118/1.4955436, URL https://onlinelibrary.wiley.com/doi/abs/10.1118/1.4955436. _eprint: https://aapm.onlinelibrary.wiley.com/doi/pdf/10.1118/1.4955436.

[34] G. Pinton, J.-F. Aubry, M. Fink, M. Tanter, Effects of nonlinear ultrasound propagation on high intensity brain therapy, Med. Phys. 38 (3) (2011) 1207–1216, http://dx.doi.org/10.1118/1.3531553, URL https://onlinelibrary.wiley.com/doi/abs/10.1118/1.3531553. _eprint: https://onlinelibrary.wiley.com/doi/pdf/10.1118/1.3531553.

[35] G. Pinton, J.-F. Aubry, E. Bossy, M. Muller, M. Pernot, M. Tanter, Attenuation, scattering, and absorption of ultrasound in the skull bone, Med. Phys. 39 (1) (2012) 299–307, http://dx.doi.org/10.1118/1.3668316, URL https://onlinelibrary.wiley.com/doi/abs/10.1118/1.3668316. _eprint: https://onlinelibrary.wiley.com/doi/pdf/10.1118/1.3668316.

[36] Y. Younan, T. Deffieux, B. Larrat, M. Fink, M. Tanter, J.-F. Aubry, Influence of the pressure field distribution in transcranial ultrasonic neurostimulation, Med. Phys. 40 (8) (2013) 082902, http://dx.doi.org/10.1118/1.4812423.

[37] Z. Xu, C. Carlson, J. Snell, M. Eames, A. Hananel, M.B. Lopes, P. Raghavan, C. Lee, C. Yen, D. Schlesinger, N.F. Kassell, J. Aubry, J. Sheehan, Intracranial inertial cavitation threshold and thermal ablation lesion creation using MRI-guided 220-kHz focused ultrasound surgery: preclinical investigation, J. Neurosurg. 122 (1) (2015) 152–161, http://dx.doi.org/10.3171/2014.9.JNS14541.

[38] R.P. Williams, J.C. Simon, V.A. Khokhlova, O.A. Sapozhnikov, T.D. Khokhlova, The histotripsy spectrum: differences and similarities in techniques and instrumentation, Int. J. Hyperth. 40 (1) (2023) 2233720, http://dx.doi.org/10.1080/02656736.2023.2233720, Publisher: Taylor & Francis _eprint: https://doi.org/10.1080/02656736.2023.2233720.

[39] M.M. Karzova, et al., Shock formation and nonlinear saturation effects in the ultrasound field of a diagnostic curvilinear probe, J. Acoust. Soc. Am. 141 (4) (2017) 2327–2337, http://dx.doi.org/10.1121/1.4979261.

[40] W. Kreider, P.V. Yuldashev, O.A. Sapozhnikov, N. Farr, A. Partanen, M.R. Bailey, V.A. Khokhlova, Characterization of a multi-element clinical HIFU system using acoustic holography and nonlinear modeling, IEEE Trans. Ultrason. Ferroelectr. Freq. Control 60 (8) (2013) 1683–1698, http://dx.doi.org/10.1109/TUFFC.2013.2750.

[41] E. Martin, D. Jeanmonod, A. Morel, E. Zadicario, B. Werner, High-intensity focused ultrasound for noninvasive functional neurosurgery, Ann. Neurol. 66 (6) (2009) 858–861, http://dx.doi.org/10.1002/ana.21801.

[42] D. Jeanmonod, B. Werner, A. Morel, L. Michels, E. Zadicario, G. Schiff, E. Martin, Transcranial magnetic resonance imaging-guided focused ultrasound: noninvasive central lateral thalamotomy for chronic neuropathic pain, Neurosurg. Focus. 32 (1) (2012) E1, http://dx.doi.org/10.3171/2011.10.FOCUS11248.

[43] A.Y. Ammi, T.D. Mast, I.H. Huang, T.A. Abruzzo, C.-C. Coussios, G.J. Shaw, C.K. Holland, Characterization of ultrasound propagation through *Ex-vivo* human temporal bone, Ultrasound Med. Biol. 34 (10) (2008) 1578–1589, http://dx.doi.org/10.1016/j.ultrasmedbio.2008.02.012, URL https://www.sciencedirect.com/science/article/pii/S0301562908000938.

[44] O.A. Sapozhnikov, S.A. Tsysar, V.A. Khokhlova, W. Kreider, Acoustic holography as a metrological tool for characterizing medical ultrasound sources and fields, J. Acoust. Soc. Am. 138 (3) (2015) 1515–1532, http://dx.doi.org/10.1121/1.4928396.

[45] B. Treeby, F. Lucka, E. Martin, B.T. Cox, Equivalent-source acoustic holography for projecting measured ultrasound fields through complex media, IEEE Trans. Ultrason. Ferroelectr. Freq. Control 65 (10) (2018) 1857–1864, http://dx.doi.org/10.1109/TUFFC.2018.2861895.